A novel glue attachment approach for precise anchoring of hydrophilic EGCG to enhance the separation performance and antifouling properties of PVDF membranes

A novel glue attachment approach for precise anchoring of hydrophilic EGCG to enhance the separation performance and antifouling properties of PVDF membranes

Guo-Liang Zhuang [a,b], Lei-Chia Wang [c], Yi-Chen Lin [c,d], Jing-Yi Li [a],
Katerina Setnickova [e], Hui-Hsin Tseng [a,c,*]

[a] *Department of Environmental Engineering, National Chung Hsing University, Taichung 402, Taiwan*
[b] *School of Engineering, University of Edinburgh, Robert Stevenson Road, Edinburgh EH9 3FB, United Kingdom*
[c] *School of Occupational Safety and Health, Chung Shan Medical University, Taichung 402, Taiwan*
[d] *School of Chemical and Biomolecular Engineering, The University of Sydney, New South Wales 2006, Australia*
e Department of Bioorganic Compounds and Nanocomposites, The Czech Academy of Sciences, Institute of Chemical Process Fundamentals, Rozvojova 135, 16502 Prague 6, Czech Republic

Corresponding authors:
* Department of Environmental Engineering, National Chung Hsing University, Taichung 402, Taiwan.
Tel. : +886-4-22840441 ext. 508; fax: +886-4-22862587.
E-mail address: hhtseng@nchu.edu (H.-H. Tseng)

Abstract

A novel glue attachment approach was proposed to form a durable hydration layer on a hydrophobic PVDF hollow fiber membrane (PVDF HFM) surface to improve its hydrophilicity and antifouling ability during wastewater filtration. The functional glue was synthesized from reclaimed styrene butadiene rubber (SBR) and a hydroxyl group was created with an epoxidation reaction (ESBR). The hydrophilic epigallocatechin-s-gallate (EGCG) was then precisely anchored via hydrogen bonding with multiple phenolic hydroxyl groups in the ESBR without penetrating into the inner matrix of the PVDF to prevent flux decline. The hydrophilicity of the PVDF membrane increased drastically and the water contact angle decreased from 62.7° to 45.1° with only a 25% decline in the pure water flux. Furthermore, due to precise anchoring of the EGCG, the modified EGCG-ESBR/PVDF membrane showed a higher pure water flux (110.6 L m^{-2} h^{-1}) and much higher BSA and oil (kerosene) rejection rates (approximately 94.5% and 99.5%, respectively) compared to membranes directly coated with EGCG (EGCG-PVDF). Moreover, the modified membrane also showed higher water flux recovery after multiple filtration cycles. This promising and efficient hydrophilic modification suggests great potential for application of the eco-friendly material in wastewater treatment.

Keywords: Hydrophilic surface modification; Reclaimed rubber; Epigallocatechin gallate; Hydrogen bond; Anti-fouling performance

1. Introduction

Membrane filtration is a renewable technique for treating effluent containing small and nondegradable contaminants after biological treatment processes, and it features low energy consumption, an environmentally friendly process, and ease of operation [1, 2]. With the development of membrane technology, various functional materials are emerging for wastewater treatment. As a desirable material, polyvinylidene fluoride (PVDF)-based ultrafiltration (UF) membranes have been widely applied in various industries, such as the dairy industry (biomacromolecule filtration) and oil-water suspension applications, because of their excellent mechanical strength, superior thermal stability and good chemical properties [3]. However, the intrinsic hydrophobic property of PVDF membranes is the major barrier. Serious fouling easily occurs on the membrane surface due to the attraction of biometrics, such as proteins and organic species, resulting in a high frequency of membrane cleaning, performance decline, and lifetime shortening [4, 5]. In this regard, many experts are devoted to developing new strategies for achieving high permeability and excellent anti-fouling ability in real

applications.

Hydrophilic surface modification is a known method for enhancing the performance of PVDF membranes by linking the hydrophilic modifier onto the membrane surface via physical coating/deposition [6-8] and chemical bonding [9-13], such as molecules with functional groups (hydroxyl, amine and sulfonic acid groups: PEG, PVA, PVP, PEGMA, chitosan, catechin, dopamine, trimethoxysilane, etc. [14-23]. The modification solution generally treats the membrane via the dip coating or immersion method [24, 25], which have reduced likelihood of defect formation in the membrane matrix compared to conventional methods (such as the blending method [26-29]). Despite these positive developments, a few challenges remain, especially a negative effect on permeability. Sun and Feng [30] prepared a high rejection of amine-modified membranes by doping an amine solution. These membranes exhibited better surface hydrophilicity but significantly lower water permeability due to the blocking of pores in the membrane. Wang et al. [8] developed a strategy for coating functional cellulose molecules on PVDF membranes, which improved the hydrophilicity and antifouling performance of membranes used in protein filtration. However, over-aggregation of the cellulose molecules occurred inside the membrane pores, negatively impacting water permeability due to the narrow pathway. As discussed above, surface hydrophilic modification generally leads to a decline in water permeance due to the

denser structure formed by an extra layer on the membrane surface or inside the pores.

In addition, the chemical processability of the PVDF membrane should be considered. Several studies have attempted to modify the molecular structures of PVDF membranes directly with grafting methods designed to effectively improve the surface hydrophilicity and separation performance. However, the stable PVDF molecular chains must be activated first by forming hydroxyl groups with, for example, alkali treatment [22, 31] and irradiation treatment (UV, plasma and high-energy electron beam) [3, 32, 33]. The pretreatment process is required for the grafting reaction of the PVDF membrane, which could limit development due to the complicated and expensive process. Therefore, to overcome these shortcomings, it is necessary to develop an environmentally friendly, low-cost, and sustainable hydrophilic modification technology to expand the application potential.

To address these issues, we designed a novel, facile and effective surface modification method for fabricating a highly hydrophilic and anti-fouling PVDF HFM using eco-friendly and inexpensive materials and a green glue attachment approach. Plant-derived epigallocatechin-3-gallate (EGCG) is one of the major tea catechins in green tea extracts and is a common polyphenol material, and it exhibits good hydrophilicity due to the abundance of hydroxyl groups [34, 35]. To deposit EGCG onto the PVDF membrane surface controllably without penetrating the inner matrix, we

sought to design a glue layer to react with EGCG via hydrogen bonding. Reclaimed styrene butadiene rubber (SBR) derived from waste tires was used as the glue precursor.

As shown in Scheme 1, the glue precursor SBR was first coated onto the PVDF HFM surface and went through the epoxidation reaction with peroxyformic acid to form an epoxidized layer ESBR. The ESBR shows high thermal stability and hydrophilicity due to the oxirane group [36, 37]. The epoxide (oxirane ring) group in this ESBR layer is transformed to a hydroxyl group under basic conditions when the EGCG is added, which functions as a precise anchor for the *in situ* reaction with EGCG. Thus, in this reaction, hydrophilic EGCG was effectively reacted with ESBR through multiple hydrogen bonds between the hydroxyl groups of ESBR and the phenolic hydroxyl groups in EGCG. The ESBR acts as a functional glue layer to react precisely with EGCG to form a hydrophilic layer on the membrane surface without clogging its inner pores. Moreover, the strength of this interaction between EGCG and ESBR could endow the modified membrane with a durable performance during the filtration process. Thus, in this work, the time required for the epoxidation reaction was optimized, and the effects of the modified membrane on the filtration efficiencies for separation of proteins and oily pollutants from wastewater were evaluated.

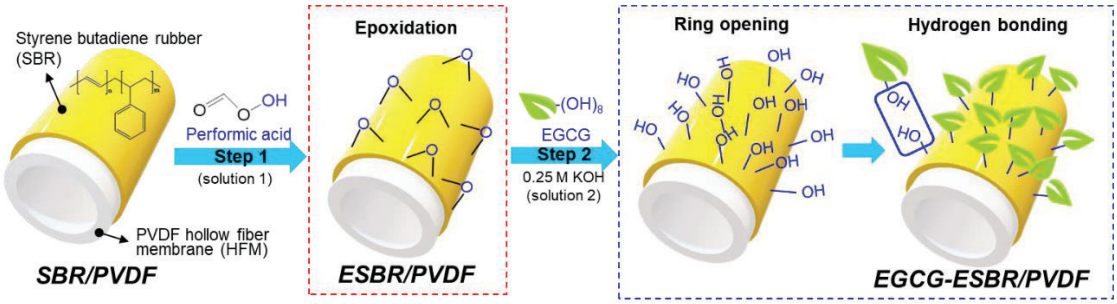

Scheme 1. Schematic illustration of the fabrication of the EGCG-ESBR/PVDF membrane via the *in situ* modification approach.

2. Experimental

2.1 Material

A commercial hollow fiber PVDF membrane was obtained from Ray-E Creative Co., Ltd. (Taipei, Taiwan), and the examined PWF was ~150 L/m^{2}h, the BSA rejection was approximately 90%, and the flux recovery rate was 80.2%. Styrene butadiene rubber (SBR) was fully regenerated from discarded inner tires [38]. Toluene (purity of 99.8%), methanol (purity of 99.9%), ethanol (EtOH, purity of 99.8%), Tween 60 (purity of 100%), kerosene (purity of >99%) and oil red O (MW = 408.49 g/mol) were purchased from Sigma–Aldrich. Reagent grade potassium hydroxide (KOH, purity of 85%) was supplied by Duksan Pure Chemicals Co. Ltd.

Bovine serum albumin (BSA) (MW = 67,000 g/mol), which was purchased from Sigma Aldrich, was used as a model protein foulant. The BSA feed was prepared in phosphate-buffered saline (PBS) solution (pH = 7) at a concentration of 1.0 mg/ml. EGCG (purity of >98%) was provided by TCI (Shanghai) Development Co. Ltd.

2.2 Fabrication of the hollow fiber SBR/PVDF composite membrane

The SBR glue layer on the PVDF HFMs was prepared by a vacuum-assisted dip-coating method [39] and a nonsolvent-induced phase separation (NIPS) process. As shown in Fig. 1, 3 wt.% SBR was first introduced into toluene and magnetically stirred overnight until the solutions were homogeneous (the optimal SBR concentration was chosen by the water permeance test and SEM surface image observed, as shown in Fig. S1). Two end sides of the dried PVDF membranes sealed with an epoxy resin were coated with SBR solution by the dip-coating method at an immersion and withdrawal rate of 120 mm/min at a vacuum degree of 1.0 atm for 30 s. Next, the membranes were immersed in a coagulating bath (with the concentration of EtOH in water ranging from 0－100 vol%) for phase inversion and then treated with methanol and n-hexane to completely remove the residual solvent by solvent exchange. Finally, the composite membranes were dried under ambient conditions and employed in the hydrophilic

161 modification process.

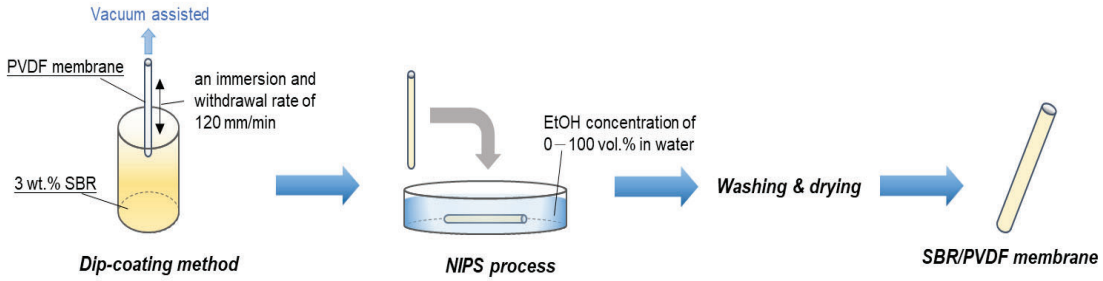

162

163 **Fig. 1.** Preparation of the SBR/PVDF membrane by nonsolvent-induced phase

164 separation.

165

166 *2.3 Hydrophilic modification processes*

167

168 The surface of the SBR/PVDF composite membrane was further modified with

169 hydrophilic chemical groups. The modification included a two-step reaction: (1) the

170 SBR skin layer of the composite membrane was epoxidized to form the ESBR/PVDF

171 membrane, and then (2) EGCG was coated onto the membrane surface via *in situ*

172 deposition to prepare the EGCG-ESBR/PVDF membrane. Table S1 summarizes the

173 fabrication conditions of the resulting membranes via the aforementioned modification

174 processes.

175 In the first step, the SBR intermediate layer was epoxidized *in situ* with an aqueous

176 mixture of formic acid (>98 vol%) and hydrogen peroxide (30 vol%) with a mole ratio

177 of 1.5. The dried SBR/PVDF membranes were immersed in the mixture for 0.5-3 h,

178 and the excess solution was drained to obtain the ESBR/PVDF membrane. Next, the
179 EGCG was dissolved in a 0.25 M KOH solution at 85 °C overnight and magnetically
180 stirred to obtain a homogeneous coating solution containing 0.1 mg/ml EGCG. The
181 pristine membrane or the epoxidized membranes were immersed in the EGCG solution,
182 and the deposition reaction was performed for 2 to 12 h. The membrane was then
183 washed with distilled water until a neutral pH was reached. Afterward, the membranes
184 were dried overnight in an oven at 60 °C to obtain the EGCG-PVDF membrane or
185 EGCG-ESBR/PVDF membrane.
186
187 *2.4 Characterization methods*
188
189 The surface morphologies and the elemental maps of the membranes were
190 observed with field emission scanning electron microscopy (FE-SEM; Model JEOL
191 JSM-6700F from Hitachi Co., Japan) and an energy dispersive X-ray (EDX) detector,
192 respectively. The surface hydrophilicity of the membranes was determined by a contact
193 angle (CA) measuring instrument (KRÜSS Instruments, Mobile Drop GH11). All
194 reported CA data were obtained by using the sessile drop technique with deionized
195 water droplets; an average of three drops was applied to each surface. The surface
196 roughnesses of the membrane were analyzed by atomic force microscopy (AFM;

Bruker Dimension Icon, Bruker, MA, USA). The chemical structure of the membranes was measured by attenuated total reflectance Fourier transform infrared (ATR-FTIR) spectroscopy using an FTIR-4100 spectrophotometer (JASCO, USA). All transmission spectra were recorded in the range of 4000–600 cm^{-1} at a scanning rate of 10 kHz with a total of 16 scans. The molecular weight cutoffs (MWCOs) of the membranes were assessed with rejection of polyethylene glycol (PEG) solutes with various molecular weights ranging from 1 to 300 kDa in a 500 mg L^{-1} feed solution. A photometer (WTW, photoLab® S6, Germany) was used to determine the PEG concentrations of the feed solutions and the permeate after filtration for 1 h. The rejection rate for each solute was calculated with equation (2) and plotted against the molecular weight. Finally, the MWCO of the membrane was estimated from 90% solute removal.

2.5 Assessment of filtration and antifouling performance

A lab-scale cross-flow filtration system step-up was used to evaluate the permeation and separation performances of the fabricated membranes. A membrane module consisting of a fiber with an effective length of 10 cm was used. The hollow fiber membranes were initially prepared by using deionized water at 2.5 bar for 30 min in advance of the test. After compaction, the pure water flux (PWF, J_w, L m^{-2} h^{-1}) was

measured under a pressure of 2 bar and calculated with equation (1) [40]:

$$PWF\ (J_w, \mathrm{L{\cdot}m^{-2}{\cdot}h^{-1}}) = \frac{V}{A \cdot \Delta t} \quad (1)$$

where V is the volume of permeate (L) collected in the determined time interval, Δt (h), and A is the effective membrane area (m^2).

A filtration test with a model foulant was subsequently performed to measure the anti-fouling properties of the resulting membrane. The foulant feed included both 1 mg/ml BSA aqueous solution for protein filtration studies and 1 mg/ml Tween 60-stabilized kerosene-in-water emulsions for the oil/water separation studies. During filtration, the permeate flux (J_f) was measured. The foulant rejection (R) was obtained by using a UV–visible spectrophotometer (U-3900 Spectrophotometer from Hitachi Co., Japan) to analyze the concentrations of foulant in the feed (C_f, mg/L) (wavelength at 280 nm for BSA protein, at 518 nm for oil red O) and the collected permeate (C_p, mg/L), and R was calculated with equation (2) [41]:

$$Rejection\ (R, \%) = \frac{C_f - C_p}{C_f} \times 100\% \quad (2)$$

After filtration, the membranes were cleaned by backwashing with pure water for 30 min. The pure water flux ($J_{w'}$) of the cleaned membrane was then reevaluated. To determine the antifouling properties of the membranes during the filtration process, the membrane fouling (R_m), total fouling (R_t), and irreversible and reversible fouling (R_{ir} and R_r) were calculated with equations (3), (4), (5), and (6), respectively [42]:

$$Membrane\ fouling\ (R_m, \mathrm{m^{-1}}) = \frac{\Delta P}{\mu \times J_w} \quad (3)$$

$$Total\ fouling\ (R_t, \mathrm{m^{-1}}) = \frac{\Delta P}{\mu \times J_f} \quad (4)$$

$$Irreversible\ fouling\ (R_{ir}, \mathrm{m^{-1}}) = \frac{\Delta P}{\mu \times J_{w'}} \quad (5)$$

$$Reversible\ fouling\ (R_r, \mathrm{m^{-1}}) = R_t - R_m - R_{ir} \quad (6)$$

where ΔP is the transmembrane pressure (Pa); μ is the permeate viscosity (Pa s); $J_{w,1}$ is the PWF before foulant filtration; and the flux recovery rate (FRR), total flux decline ratio (FDR) and irreversible flux decline ratio (DR_{ir}) were calculated with equations (7), (8), and (9), respectively [43]:

$$FRR\ (\%) = \frac{J_{w,2}}{J_{w,1}} \times 100\% \quad (7)$$

$$FDR\ (\%) = \left(1 - \frac{J_f}{J_{w,1}}\right) \times 100\% \quad (8)$$

$$DR_{ir}\ (\%) = \left(1 - \frac{J_{w,2}}{J_{w,1}}\right) \times 100\% \quad (9)$$

3. Results and discussion

3.1 Characterization and separation performance of the SBR/PVDF composite membrane

To investigate the influence of nonsolvents on the surface morphology of the membranes in the NIPS process, AFM and FE-SEM were used to evaluate the surface properties of the composite SBR/PVDF membranes (Fig. 2). The SBR glue layer fabricated in the nonsolvent with a low EtOH concentration (a and b) had an irregular surface structure, and macropores were observed. Fig. 2c-e shows the membranes using a 50 vol% and 75 vol% EtOH-water mixture and pure EtOH as nonsolvents. The surface became smoother, and the size and quantity of pores were reduced with increasing EtOH concentration. Similar results were obtained from AFM images of the change in surface roughness (Fig. 2f-j). The average roughness (Ra) of the membrane surface decreased as the EtOH concentration was increased. The presence of EtOH in a nonsolvent can lead to the formation of a relatively smooth membrane surface. The obtained surface morphologies were in good agreement with the results of the protein separation experiment.

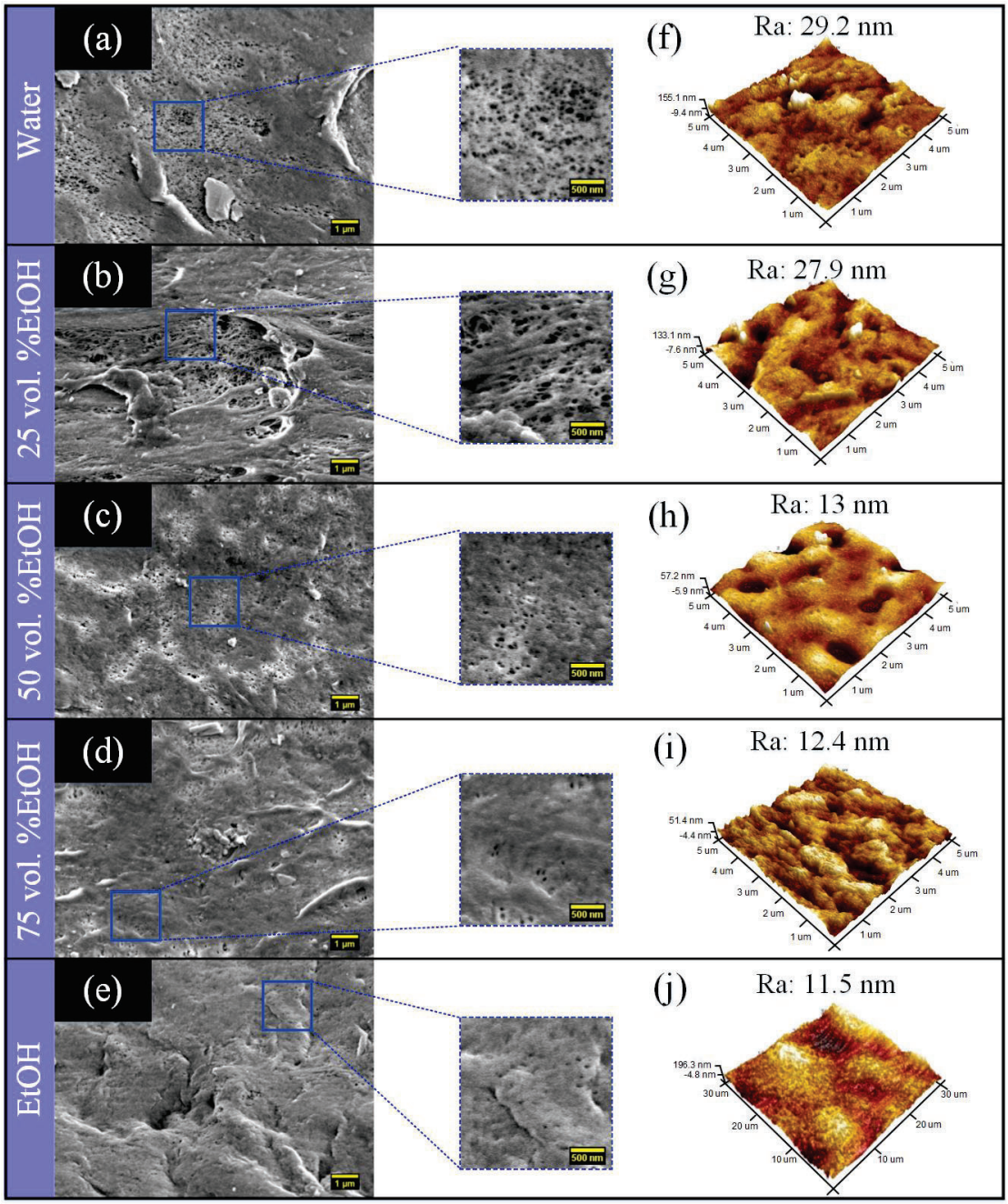

Fig. 2. FE-SEM and AFM images of the composite SBR/PVDF membranes coagulated in different nonsolvent baths. (a and f): deionized water; (b and g) 25 vol %EtOH: 75 vol % water; (c and h) 50 vol % EtOH: 50 vol % water, (d and i) 75 vol % EtOH: 25 vol % water and (e and j) EtOH.

Solubility in a solvent may affect the liquid–liquid demixing speed during phase inversion [44]. The miscibility of the solvent and nonsolvent affects membrane formation, which can be determined by calculating the difference in the solubility parameters (δ, $MPa^{1/2}$) of the solvent and nonsolvent. The following equation can be used to predict the interaction parameters between solvent and nonsolvent [45]:

$$\delta_t = \sqrt{\delta_d^2 + \delta_p^2 + \delta_h^2} \quad (10)$$

$$\delta_d = x_1\delta_{d1} + x_2\delta_{d2} \quad (11)$$

$$\delta_p = x_1\delta_{p1} + x_2\delta_{p2} \quad (12)$$

$$\delta_h = x_1\delta_{h1} + x_2\delta_{h2} \quad (13)$$

where δ_t is the total solubility parameter, and the contribution can be divided into three parts: dispersion force (δ_d), polar force (δ_p) and hydrogen bonding force (δ_h); x_i is the volume fraction of chemical compound i. The solubility parameters of toluene and nonsolvent are presented in Table 1.

The difference in solubility parameter, $\Delta\delta_{toluene\text{-}NS}$, between the toluene of the dip-coating dope and the nonsolvent system of the coagulating bath can be further calculated:

$$\delta_{toluene-NS} = \sqrt{\left[\left(\delta_{d,toluene} - \delta_{d,NS}\right)^2 + \left(\delta_{p,toluene} - \delta_{p,NS}\right)^2 + \left(\delta_{h,toluene} - \delta_{h,NS}\right)^2\right]} \quad (14)$$

As shown in Table 1, the solubility difference decreased with increasing EtOH concentration in the nonsolvent. The results were correlated with the surface structure of the membranes (shown in Fig. 2), and the higher solubility difference resulted in the formation of a macroporous structure. In contrast, a lower solubility difference caused the formation of a denser structure. In other words, the microporous structure can be inhibited by controlling the EtOH concentration in a nonsolvent. A similar change in the surface morphologies of the rubber membranes in the EtOH-water nonsolvent mixture was observed by Kuźmińska et al. [46]. Ren et al. [47] also studied the effect of EtOH on the membrane microstructure and concluded that the diffusivity in the solvent–nonsolvent system is a major controlling factor in the formation of the pore structure.

Table 1 The solubility parameter (δ) in toluene solvent [48] and various nonsolvents [49]; differences in the solubility parameter in toluene–nonsolvent ($\delta_{toluene\text{-}NS}$)

Chemical compound	Solubility parameter ($MPa^{1/2}$)				$\sqrt{\sum(\Delta\delta_{toluene-NS})^2}$
	δ_t	δ_d	δ_p	δ_h	
Toluene	18.2	18.0	1.4	2.0	-
H_2O	47.8	15.6	16.0	42.3	42.9
25% EtOH	42.2	15.7	14.2	36.6	36.9
50% EtOH	36.8	15.7	12.4	30.9	31.0
75% EtOH	31.5	15.8	10.6	25.1	25.0
EtOH	26.5	15.8	8.8	19.4	19.0

The pure water flux (PWF) and separation performance of the composite SBR/PVDF membranes fabricated in the different nonsolvents are shown in Fig. 3. The

296 composite membranes coagulated in the mixtures with low EtOH concentrations (0
297 vol.%, 25 vol.% and 50 vol.%) had a higher pure water flux, approximately 101-105 L
298 m^{-2} h^{-1}, while the mixtures with higher EtOH concentrations showed a significant
299 decrease in pure water flux. However, the results of protein separation presented a
300 different flux trend. The permeate flux of the membranes increased with the
301 concentration of EtOH, while the permeate flux showed a maximum value of 82 L m^{-2}
302 h^{-1} at 50 vol.% EtOH and then decreased to 50.3 L m^{-2} h^{-1} at 75 vol.% EtOH and 34.1 L
303 m^{-2} h^{-1} in pure EtOH. However, the BSA rejections of the different composite
304 membranes were nearly the same, approximately 95% or above, possibly because the
305 pore sizes of the membranes were all smaller than the BSA size.

306 There are two main reasons for the difference in the flux trend of pure water and
307 permeate. First, the high permeability of the membranes was in good agreement with
308 their macropores on the surface of the membrane, as confirmed by the SEM images
309 (Fig. 2) and mean pore size (Table 1). In contrast, further increases in the EtOH
310 concentration led to dense surface formation, resulting in a decrease in pure water flux.
311 Second, the higher roughness of the membranes, as noted recently by researchers [50],
312 can easily cause the penetration/adhesion of foulants on the rough surface. Therefore,
313 the resulting membrane at low EtOH concentrations had a lower permeate flux due to
314 fouling formation. According to the above results, a comparison of all membranes

showed that 50 vol.% EtOH was the most preferred choice as a nonsolvent because it led to a smoother surface with a relatively higher porosity, so it was used to fabricate subsequent membranes for hydrophilic modification.

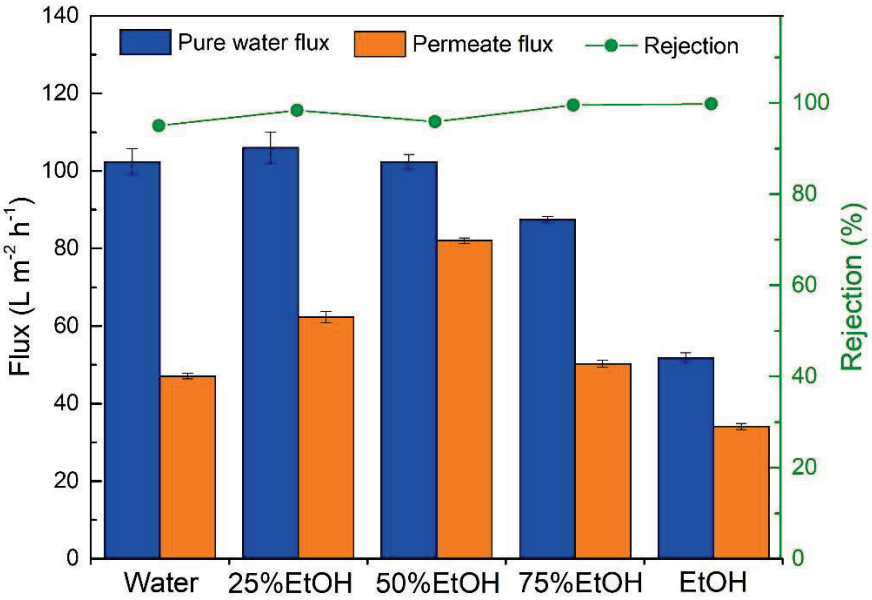

Fig. 3. Fluxes and protein filtration efficiencies of the composite SBR/PVDF membranes coagulated in different nonsolvent baths.

3.2 Effect of the EGCG coating on the hydrophilic modification of the EGCG-ESBR layer

As shown in Fig. 4a, variations are apparent in the carbon double bond (C = C) adsorption peak at 971 cm^{-1}. This peak started at a maximum value and then decreased during the epoxidation process until it was completely lost from the reaction. The oxirane groups had relatively weaker adsorption at 1183 cm^{-1}, corresponding to the stretching of C–O–C, which increased with the epoxidation time. The adsorption of the C=O groups at 1717 cm^{-1} increased simultaneously due to the side reaction that took place during the epoxidation reaction [36].

We examined the optimal reaction time for modifying the surface hydrophilicities of the membranes and estimated it with the water contact angle (WCA) of the membrane surface, as shown in Fig. 4b. The pristine SBR/PVDF composite membrane had a high WCA of 99%. With the increase in the reaction time, the WCA of the modified membranes (ESBR/PVDF) dramatically decreased to 68.2° until the reaction time for the epoxidation reaction reached 1.5 h. The decrease in WCA occurred because the hydrophilic oxirane group was formed on the epoxidized membrane surface. Nevertheless, the WCA remained constant when the reaction time was extended to 3 h. Thus, the optimal epoxidation time of the ESBR/PVDF membrane was 1.5 h, and this

was used for the next modification step.

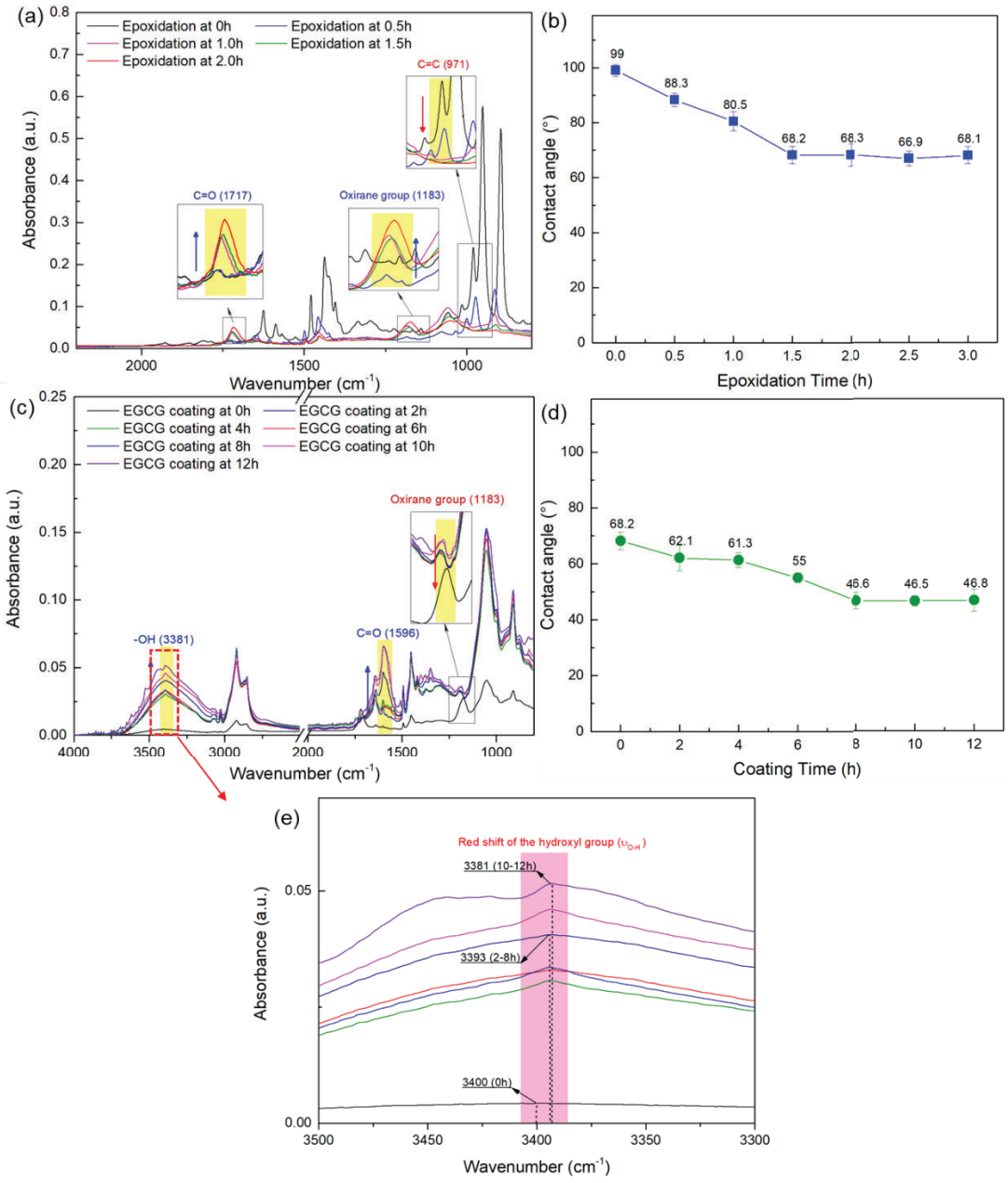

Fig. 4. Changes in the (a, c) ATR-FTIR spectra and (b, d) water contact angle (WCA) of the composite membranes undergoing epoxidation and EGCG coating as a function of the reaction time. (e) ATR-FTIR spectra of the EGCG coating on the ESBR/PVDF membrane as a function of reaction time at wavenumbers of hydroxyl groups at 3500–3300 cm^{-1}.

In the next reaction step, the FTIR spectra of the EGCG-coated membranes (EGCG-ESBR/PVDF) made with different coating times are shown in Fig. 4c. The EGCG-coated membrane has a relatively distinct absorption peak in the range of 3800-3200 cm^{-1}, representing the stretching vibration of the OH group, and a weaker absorption peak at 1695 and 1596 cm^{-1} due to the C=O functional group [51]. Both of these bands increased in intensity with longer reaction times, verifying the presence of EGCG on the membrane surface.

Fig. 4d shows the WCAs of the EGCG-ESBR/PVDF membranes. As expected, a decreasing trend in the WCA was observed with increasing coating time from 2 h to 8 h, and the WCA of the modified membranes decreased to approximately 46° and remained constant for 8 to 12 h. Furthermore, the change trend of hydrophilicity can be proven by observing the interaction of hydrogen bonds between EGCG and ESBR in the FTIR spectra. As shown in Fig. 4e, the absorption peak of the hydroxyl group at 3400 cm^{-1} in the spectrum of the ESBR/PVDF membrane is redshifted to 3393 cm^{-1} and 3381 cm^{-1} after coating times of 2-8 h and 10-12 h, respectively. It is suggested that the combination of EGCG and ESBR shows a successful adhesive interaction of ESBR and EGCG through an effective hydrogen bond. The results showed that enhanced hydrophilicity was acquired with the increase in EGCG deposition due to the presence of a hydroxyl group on the resultant membrane surface. Therefore, 8 h is the most

appropriate coating time for fabricating a highly hydrophilic membrane.

3.3 Mechanism of the modification reaction

The possible mechanism of the proposed two-step modification reaction is illustrated in Fig. 5. In the first step, the epoxidation reaction occurs on the surface of the SBR glue layer, resulting in the formation of oxirane groups. In the second step, the basicity can first induce a ring-opening reaction of the oxirane groups of the ESBR glue to form hydroxyl groups, which react with the hydroxyl groups of EGCG during a condensation reaction (click reaction), enabling hydrogen bonding between EGCG and the membrane surfaces.

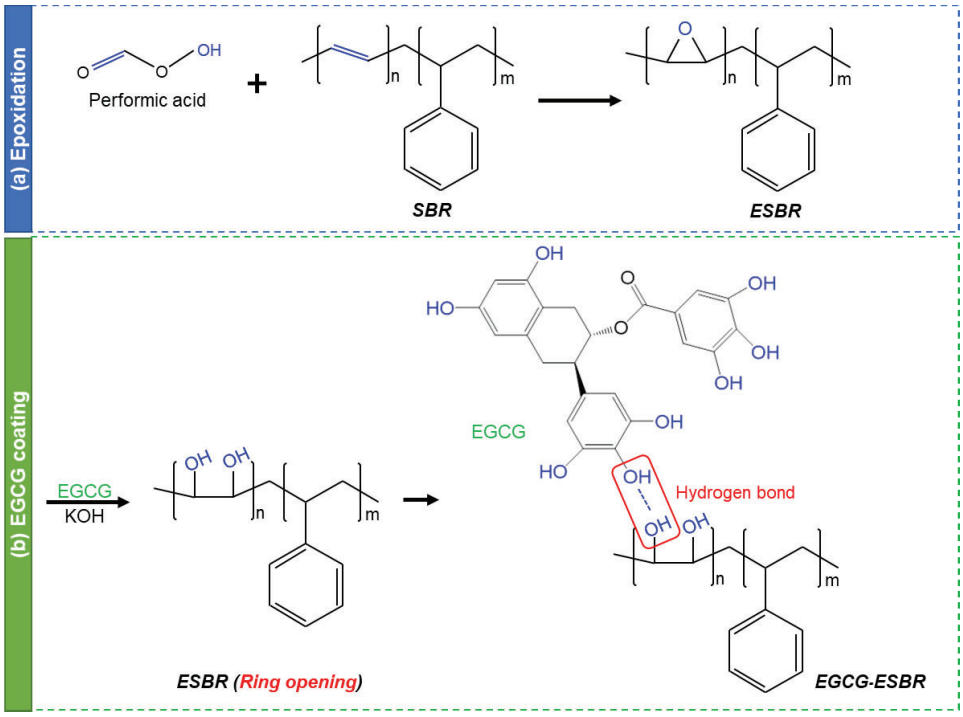

Fig. 5. Synthetic pathway for (a) the epoxidation of SBR glue and (b) coating of the EGCG.

3.4 Effect of hydrophilic modification on surface properties and separation performance

The pristine PVDF membrane was used as a model to investigate the impact of a straight EGCG coating (EGCG-PVDF) and an ESBR intermediate layer-assisted EGCG coating (EGCG-ESBR/PVDF) on the surface properties and separation performance. As shown in Fig. 6a, the presence of EGCG on the modified membranes decreased from 62.7±2° for the PVDF membrane to 50.1±1.8° and 45.1±1.9° for the EGCG-PVDF and EGCG-ESBR/PVDF membranes, respectively.

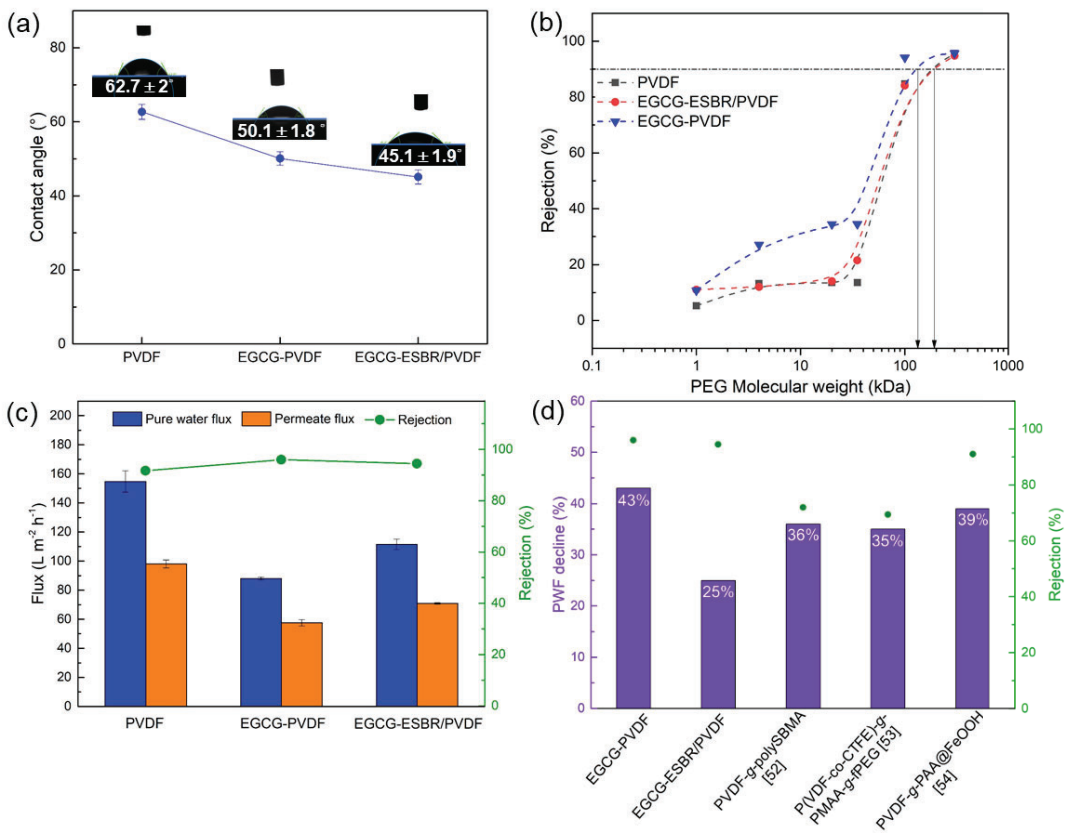

Fig. 6. (a) WCAs of the pristine and modified membranes; (b) retention curves of the resulting membranes used to determine the apparent MWCO values; (c) fluxes and BSA rejection rates of the pristine and modified membranes; (d) comparison of recently reported materials with hydrophilic-modified PVDF membranes (PVDF-*g*-polySBMA [52], both P(VDF-co-CTFE)-*g*-PMAA-*g*-fPEG [53] and PVDF-*g*-PAA@FOOH [54] in 1.0 mg/ml BSA solutions).

To determine the molecular weight cutoff (MWCO) of the pristine and modified membranes, different molecular weights of polyethylene glycols (PEGs) (1, 4, 20, 35, 100 and 300 kDa) were used as feed solutions in pressure filtration tests. As shown in Fig. 6b, all of the membranes showed MWCO values of approximately 100 to 300 kDa. The MWCO value of the EGCG-ESBR membrane was similar to that of the pristine membrane. However, the EGCG-PVDF membrane showed a lower MWCO value than the other membranes, consistent with the surface morphology observed by SEM images (Fig. S2d-f). As expected, the pore size of the membrane surface decreased when EGCG was directly coated onto the pristine membrane (Fig. S2e). In contrast, for the EGCG-ESBR/PVDF membrane, the surface morphology still maintained the pore structure after EGCG coating (Fig. S2f). As illustrated in Fig. S3, the chemical elemental compositions of the fabricated membrane were measured by using an energy

dispersive spectroscopy (EDS) unit attached to the SEM. This result clearly indicated the presence of higher O signals in the bulk of the EGCG-PVDF membrane than in the EGCG-ESBR/PVDF membrane. This result proved that the ESBR glue layer prevented deposition of the EGCG inside the pores and that an EGCG layer was efficiently deposited onto the membrane surface, which altered the surface properties.

The effect of the SBR glue layer on the hydrophilic modifications of the PVDF membrane performance is shown in Fig 6c. The PWF and BSA permeate fluxes of the EGCG-PVDF membrane were significantly decreased by 43% and 41%, respectively, compared to those of the pristine membrane. In marked contrast, the EGCG-ESBR/PVDF membrane showed only slight reductions of 25% and 26% for the PWF and permeate fluxes, respectively. Moreover, the BSA rejection rate of the membrane increased from 91.7% for the PVDF membrane to 95−96% for the EGCG-ESBR/PVDF membrane, which indicated a higher rejection rate with a lower flux decline. As shown by the above surface analyses, the coated ESBR glue layer assisted in the deposition of the EGCG selective layer on the membrane surface. Thus, EGCG effectively improved the separation performance of the PVDF membrane without a negative impact on the flux resulting from pore clogging. The performance of the modified membrane was compared to that for the hydrophilic-modified PVDF membrane, as shown in Fig. 6d. The EGCG-ESBR/PVDF membrane not only showed a lower decline in pure water

flux than the other modified membranes but also showed a competitive rejection rate during BSA filtration. More importantly, our modified membrane does not use hydrophilic modifiers, which are expensive or difficult to obtain and require cumbersome and high-energy fabrication processes. Therefore, the coated ESBR glue layer improved the pore structure and hydrophilicity of the membrane surface, which improved the permeability after modification.

3.5 Anti-fouling performance and the reliability test

To further investigate the anti-fouling properties of the membrane, the cyclic filtration performances were evaluated, as shown in Fig. 7a. During each cycle, the BSA permeate flux of the pristine and modified membranes declined rapidly at the start of filtration, especially the pristine membrane, which experienced an obvious decrease in PWF and BSA permeate flux over time during each filtration cycle. Generally, rejected protein molecules were easily deposited on the PVDF membrane surface and even inside the membrane pores. This implied that the membrane underwent severe and irreversible membrane fouling due to adsorption/deposition of the proteins [27, 55]. Membrane fouling was aggravated, and the FRR value of the pristine membrane had

447 subsequently decreased from 95.8% to 80.2% after the fourth filtration cycle, as shown
448 in Fig. 7b.

449 Compared to the pristine membrane, the permeate flux of the modified membrane
450 can be maintained at an appropriate value during operation, especially the EGCG-
451 ESBR/PVDF membrane. In marked contrast, the EGCG-ESBR/PVDF membrane
452 showed a higher permeate flux during the fourth filtration cycle than the pristine
453 membrane (Fig. 7a). Moreover, as shown in Fig. 7b, the EGCG-PVDF membrane
454 demonstrated a similar trend in the FRR value to the pristine membrane, while the
455 EGCG-ESBR/PVDF membrane showed only a slight decrease in the FRR value from
456 99.9% to 91.1% after the fourth cycle (Fig. 7b). This was due to the introduction of the
457 ESBR glue layer, which precisely anchored the hydrophilic layer on the membrane
458 surface through hydrophilic modifications with the EGCG coating. Thus, the EGCG-
459 ESBR hydrophilic layer exhibited the benefit of flux recovery and, after BSA filtration,
460 the pure water flux of the membrane was restored to its original value by simple
461 flushing.

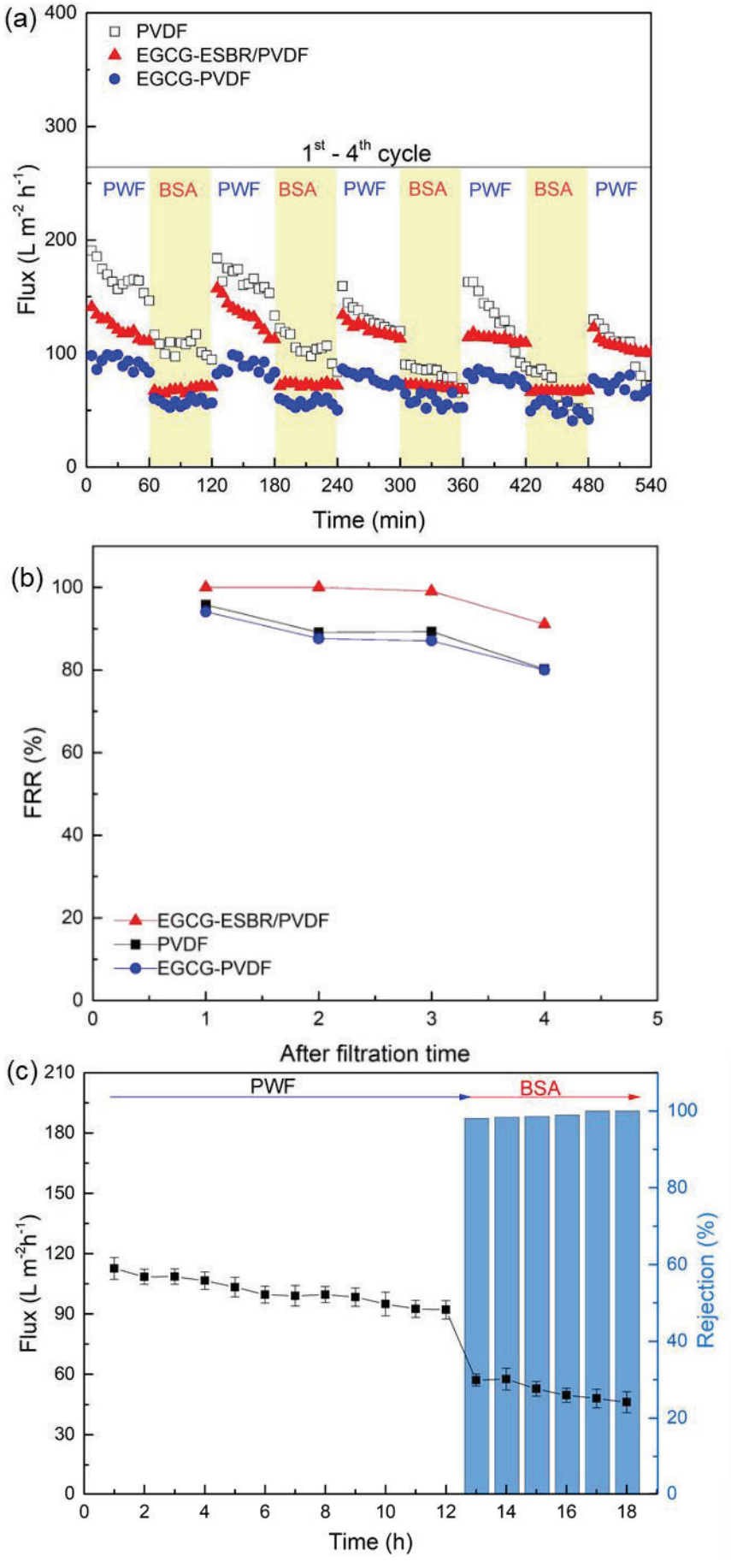
(a)
PVDF
EGCG-ESBR/PVDF
EGCG-PVDF
1st - 4th cycle
PWF
BSA
Flux (L m-2 h-1)
Time (min)
(b)
FRR (%)
EGCG-ESBR/PVDF
PVDF
EGCG-PVDF
After filtration time
(c)
PWF
BSA
Flux (L m-2h-1)
Rejection (%)
Time (h)

462

Fig. 7. (a) The fluxes of the pristine PVDF, EGCG-PVDF and EGCG-ESBR/PVDF membranes in the 4-cycle protein filtration experiments; (b) FRR values after different numbers of filtration cycles. (c) The long-term filtration stability evaluation of the EGCG-ESBR/PVDF membrane (after the cyclic filtration test) during a continuous operation for pure water permeation and BSA filtration (The membrane has been stored under atmospheric air over 6 months).

The resistance-series model was used to quantitatively analyze the antifouling properties of the membrane in detail, as shown in Fig. 8. The total resistance (R_t) of the EGCG-PVDF membrane was the highest compared to those of the other membranes due to the larger proportion of membrane resistance (R_m) at 62%. Generally, the membrane resistance to fouling depends on the surface morphologies of the membrane [56]. Thus, this result indicates that the decrease in the pore size of the membrane caused by the direct EGCG coating increases the resistance in the membrane, which could result in a dramatic decrease in the permeance of the membrane.

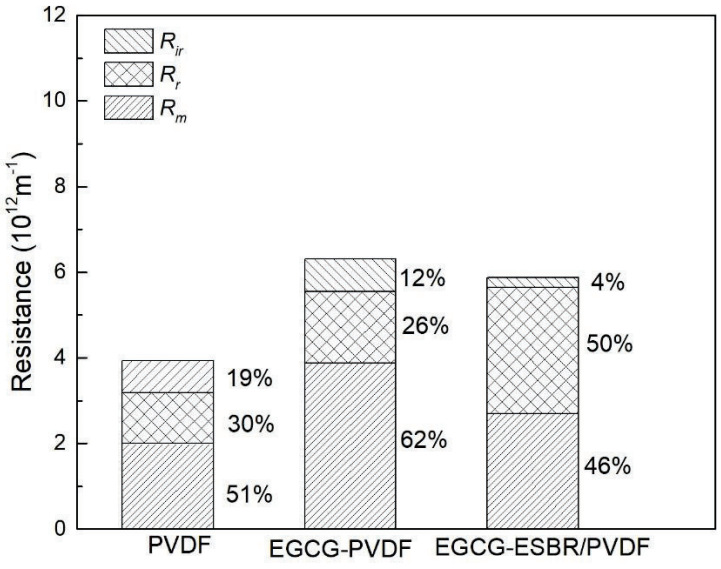

478

479 **Fig. 8.** Resistance analysis of PVDF, EGCG-PVDF and EGCG-ESBR/PVDF for BSA

480 filtration.

481 The EGCG-ESBR/PVDF membrane exhibited a higher reversible resistance (R_r)

482 of 50% and a lower membrane resistance (R_m) of 46% despite having an increase in

483 total resistance compared to the pristine membrane. Moreover, the irreversible

484 resistance (R_{ir}) significantly decreased to 4%, in contrast to that of the EGCG-PVDF

485 membrane. The surface morphologies and hydrophilic characterization results

486 confirmed that EGCG can bind onto only the near-skin layer rather than the inner-pore

487 surface during the coating process with the help of the ESBR glue on the surface of the

488 PVDF membrane. The above result was further verified by an observation of membrane

489 surface properties. The FTIR spectra and AFM images of the PVDF membrane and the

490 EGCG-ESBR/PVDF membrane are shown in Fig. 9. It can be clearly seen from FTIR

491 spectra for the fouled membranes (after the cyclic filtration test) cleaned by water, the

amide I band at 1600 to 1700 cm^{-1} was still observed on the surface of the cleaned PVDF membrane, which is related to the BSA protein residues [57]. Moreover, the surface roughness of the cleaned PVDF membrane was significantly increased to 224 nm from 109 nm of the pristine PVDF membrane. In contrast, the cleaned EGCG-ESBR/PVDF membrane didn't be observed the visible intensity of BSA protein in the FTIR spectra as well as an increase in roughness on the membrane surface after long-term operation. However, it is noteworthy that the membrane roughness has slightly decreased instead of increasing, which could be attributed to the compacted membrane during the cyclic filtration rather than the effect of residual solutes. It means that EGCG-ESBR layer is beneficial to suppressing the residual BSA protein on the membrane surface.

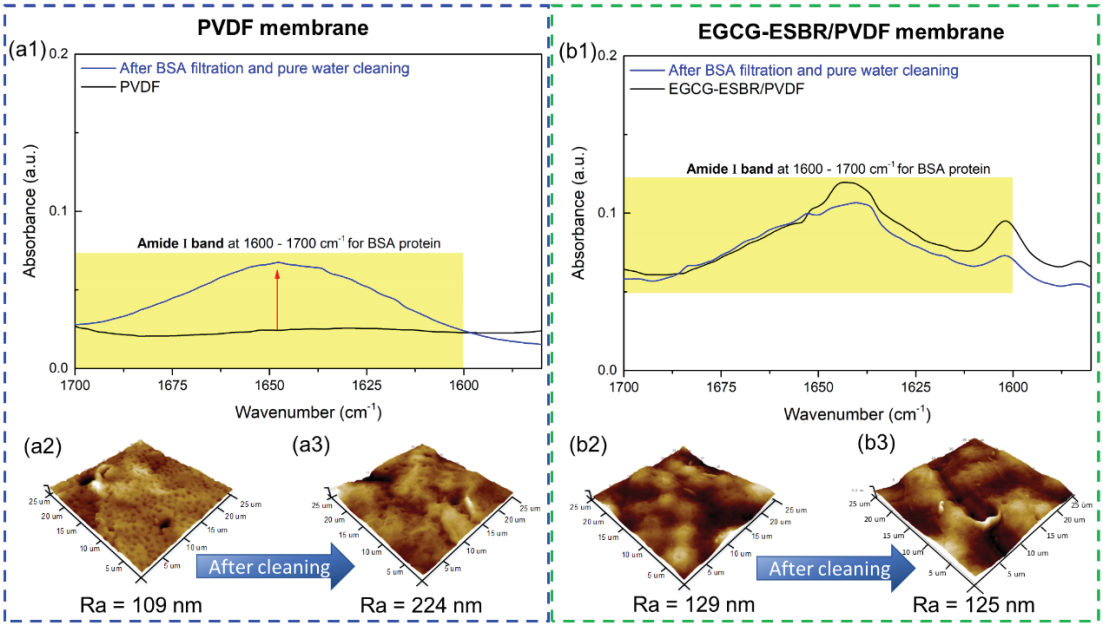

Fig. 9. FTIR spectra (a1 and b1) and AFM images (a2, 3 and b2, 3) of the PVDF and the EGCG-ESBR/PVDF membranes.

The long-term stability of the EGCG-ESBR/PVDF membrane was also further evaluated through a continuous operation time at 12 h for pure water permeation and then 6 h for BSA filtration, respectively. This membrane has been tested the cyclic filtration and then stored under atmospheric air over 6 months. As shown in Fig. 7c, the long-term stored membrane maintained a similar PWF and permeate flux after the long-term storage. Moreover, the rejection of membrane during long-term BSA filtration was a constant value of >98%. However, a slight decrease in the flux was observed during long-term operating time, which could be attributed to the transport model in the outside-in system. The membrane is expected to be more compact during the long-term operation, resulting in an increase in transport resistance. This phenomenon has been verified by the above AFM roughness observed (Fig. 7b2 and b3). Overall, although the performance was not as ideal as expected due to the operating condition limitation, the modified membrane showed good stability for long-term continuous operation.

A schematic diagram of the fouling process is displayed in Fig 10. The EGCG-PVDF membrane shows the worst surface property because of the inaccurate deposition of EGCG on the surface of the PVDF membrane. EGCG could not effectively increase

the hydrophilicity of the membrane surface due to partial permeation into the interpore of the PVDF membrane and formed the hydrophilicity/hydrophobicity of the matrix, limiting the improvement of the anti-pollution ability. Compared to the EGCG-PVDF membrane, the hydration layer was formed on the surface of the EGCG-ESBR/PVDF membrane due to the hydrophilicity of EGCG, which prevented foulants from becoming trapped or aggregating in the pores and valleys of the membrane surface. Thus, the EGCG-ESBR/PVDF membrane exhibited good separation performance and long-term anti-fouling ability due to its excellent surface properties.

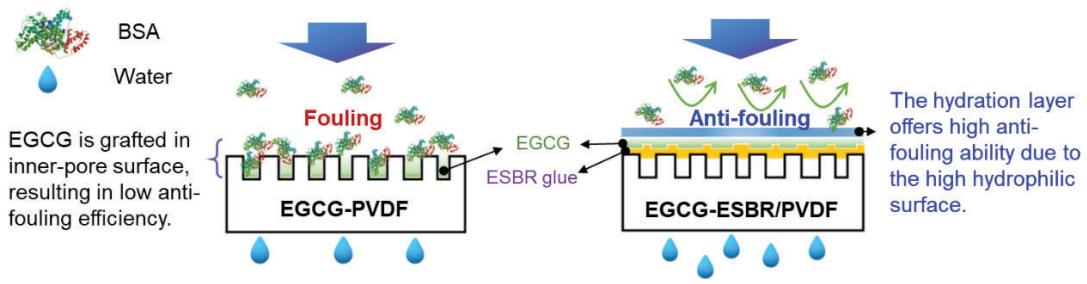

Fig. 10. Schematic illustration of the difference in the fouling process between EGCG-PVDF and EGCG-ESBR/PVDF membranes.

3.6 Oil/water emulsion separation performance

In addition, the surface hydrophilicity of the modified PVDF membrane allowed for oil-in-water emulsion separation. As shown in Fig. 11a, a similar initial pure water flux decays between the pristine membrane and the modified membrane. However, the

permeation flux of the pristine membrane dropped quickly (from 94.5 to 43.1 L m^{-2} h^{-1}) during the 60 min filtration of the oil/water emulsion. The FDR of the pristine membrane reached 55%, and the FRR recovered to 91% after cleaning Fig. 11b). In contrast, the modified membrane showed a lower decline in the permeation flux (from 65 to 47 L m^{-2} h^{-1}), the Drir was lower than 1%, and the FRR reached 99%. According to the surface wetting properties of the membrane before and after modification (Fig. 6a and Fig. 11c), greater improvements in hydrophilicity and oleophobicity were observed. This improvement occurred because of the introduction of the EGCG-ESBR selective layer on the membrane surface, which helped improve the membrane hydrophilicity.

As shown in Fig. 11d, the feeds and filtrates are displayed in the optical photographs, while many microscale droplets can be seen in the original emulsions. After filtration, no droplets could be detected in the filtered pollutants. Moreover, as shown in Fig. 11e, the modified membrane exhibited stable and high oil rejection during three-time cycle filtration. The anti-fouling performance was further proven by an underwater-oil-adhesion experiment, as shown in Fig. 11f. Compared to the EGCG-PVDF membrane, the oil droplet can remain in shape when touched and left the EGCG-ESBR/PVDF membrane rather than deform and stay on the membrane surface. It was clear that the highly hydrophilic surface of the modified membrane showed an anti-

560 fouling ability to avoid oil droplets adhering to the membrane (see the Supplementary
561 Video). This result indicated that the EGCG-ESBR/PVDF membrane successfully
562 realized oil-in-water emulsion separation and demonstrated the excellent reusability of
563 the membrane, indicating the excellent surface hydrophilicity and underwater
564 oleophobicity of the EGCG-ESBR deposited on the PVDF membrane.

565 In addition, a comparison of the comprehensive performance for newly developed
566 anti-fouling PVDF membranes reported in the literature and the fabricated membrane
567 in this work is shown in Table 2, showing that the EGCG-ESBR/PVDF membrane
568 presented promising anti-fouling performance. This result indicated that the novel
569 EGCG-ESBR layer is beneficial for enhancing the anti-fouling ability of the membrane,
570 which exhibited good reusability after recycling. In addition, this modification process
571 with the use of reuse and natural materials is not only environmentally friendly but also
572 cost-effective. As discussed above, the novel method of hydrophilic modification is
573 competitive in the separation membrane for organic wastewater treatment.

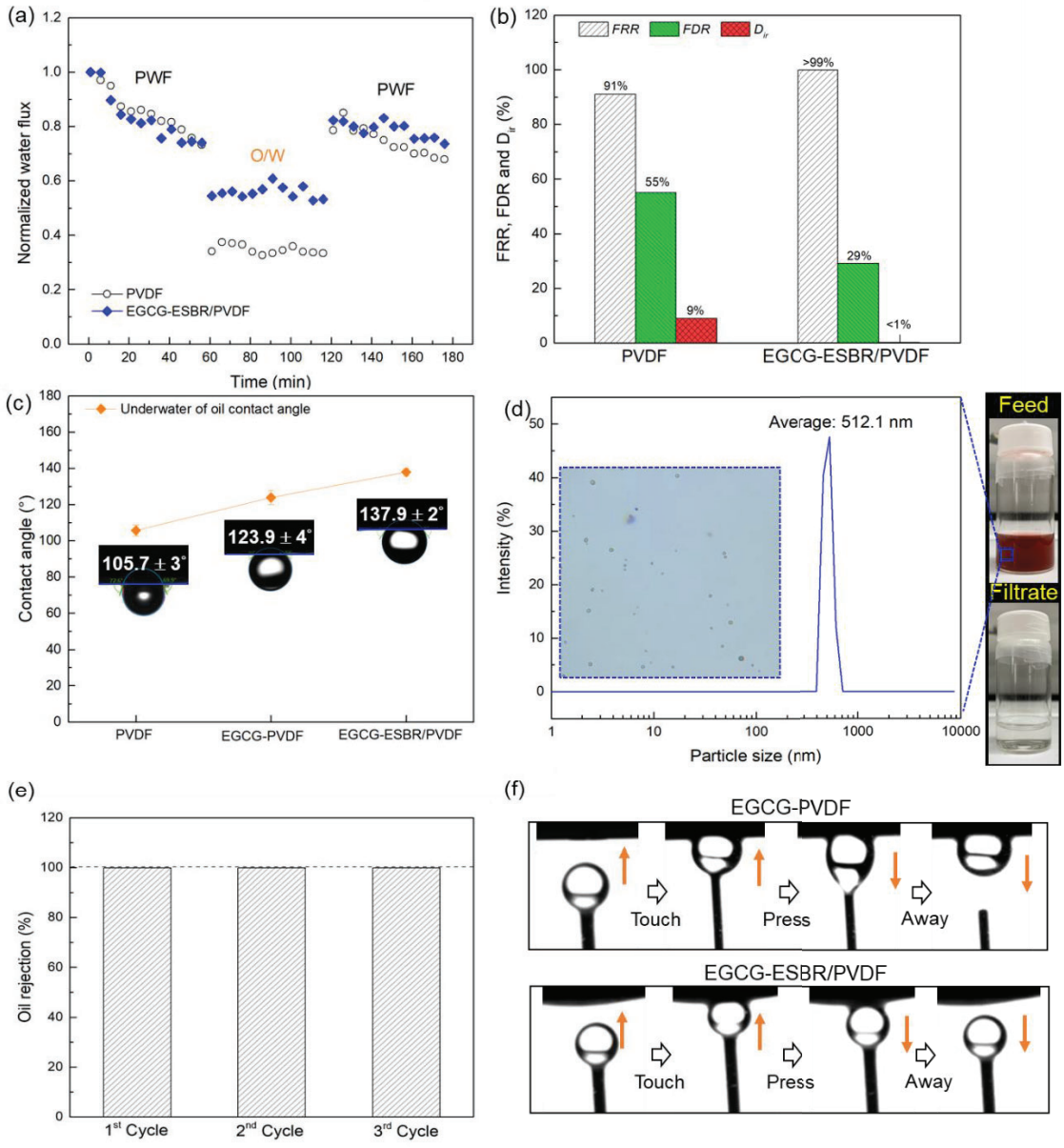

574

575 **Fig. 11.** (a) Time-dependent normalized fluxes and (b) anti-fouling properties of the

576 pristine membrane and modified membrane in the oil/water emulsion. (c) Underwater

577 oil contact angle (OCA) of the membranes. (d) Optical microscopy images before and

578 after filtration of kerosene in water. (e) The oil rejection of the modified membrane

579 after every cycle during emulsion separation. (f) Real-time recorded underwater-oil-

580 adhesion experiment on EGCG-PVDF and EGCG-ESBR/PVDF membranes.

581 **Table 2** Comparison of antif-ouling properties of the PVDF membranes for oil-in-water emulsions

Membrane	Oil-in-water emulsions	Environmentally Friendly	Recycle time	Recycle changing rate (R, %)	Rejection properties (%)	Ref.
Ag/EGCG-PVDF	SDS emulsified 0.1% diesel	Middle	5	48	>95.4	[58]
TA-Ti@PVDF	Tween 80 emulsified 1.0% petroleum ether	Middle	10	28	99.3	[59]
TA/DEDAPS PVDF	SDS emulsified 0.1% petroleum ether	Middle	6	3.7	>99.2	[60]
Cellulose-TA-PVA-PVDF	CTAB emulsified 0.2% sunflower	High	30	3.1	99.9	[61]
EGCG-ESBR/PVDF	Tween 60 emulsified 0.1% kerosene	High	3	<1	>99.5	This work

582

Conclusion

Using a green and facile approach, we designed a green EGCG-ESBR hydration layer to improve the hydrophilic surface of the PVDF membrane. To the best of our knowledge, this is the first work that reports a strategy for fabricating high anti-fouling performance membranes through glue attachment. This approach effectively prevented closing or shrinking of the pores and maintained the surface morphology while improving the membrane performance. The EGCG-ESBR/PVDF demonstrated superior protein separation performance to that of the pristine PVDF membrane. The SBR glue layer coated on the membrane surface not only reduced the surface roughness but also enhanced the precise anchoring of the hydrophilic EGCG coating. Under the optimized conditions, EGCG-ESBR/PVDF exhibited the best antifouling performance during BSA rejection (94.5%) and oil rejection (>99.5%). Moreover, the resulting membrane showed remarkable stability during multiple filtration cycles and long-term test. If desired, even higher water fluxes should be achievable by further optimizing the thickness of the glue layer on the membrane surface while using another highly hydrophilic modifier as the selective layer. In the future, reliability estimates for use with industrial wastewater and longer operating times will confirm the application potential in practical wastewater. In summary, this work provides new insights into the hydrophilic modifications of membrane surfaces for improving separation performance

602 and fouling resistance.

603

604 **Declaration of interests**

605 The authors declare that they have no known competing financial interests or
606 personal relationships that could have appeared to influence the work reported in this
607 paper.

608

609 **Acknowledgment**

610 Financial support from the Ministry of Science and Technology (MOST) in
611 Taiwan (Project numbers: MOST 109-2813-C-005-013-E, and MOST 109-2221-E-
612 005-083-MY3) is gratefully acknowledged.

613

614 **Nomenclature**

ΔP	filtration pressure (Pa)
A	effective membrane area (m^2)
BSA	bovine serum albumin
CA	contact angle
DR_{ir}	irreversible flux decline ratio
EGCG	epigallocatechin gallate
ESBR	epoxidized styrene–butadiene–styrene block copolymer membrane

FDR	flux decline ratio
FRR	flux recovery rate
J_f	permeation flux (L m^{-2} h^{-1})
J_w,	water flux (L m^{-2} h^{-1})
J_w'	water flux after cleaning (L m^{-2} h^{-1})
MWCO	molecular weight cutoff
NIPS	nonsolvent-induced phase separation
NS	nonsolvent
PET	polyethylene terephthalate
PS	polystyrene
PSF	polysulfone
PVDF	polyvinylidene fluoride
PWF	pure water flux
R	foulant rejection (%)
R_{ir}	irreversible fouling (m^{-1})
R_m	membrane fouling (m^{-1})
R_r	reversible fouling (m^{-1})
R_t	total fouling (m^{-1})
SA	sulfonic acid group
SBR	styrene–butadiene–styrene block copolymer
t	filtration time (h)
V	volume of permeate (L)
WCA	water contact angle
OCA	underwater oil contact angle
x	volume fraction

δ_d	solubility parameter of dispersion force
δ_h	solubility parameter of hydrogen bonding force
δ_p	solubility parameter of polar force
$\Delta\delta$	difference in solubility parameter
μ	permeate viscosity (Pa s)

615

616 **References**

617

618 [1] A. Mojiri, M.J. Bashir, Wastewater Treatment: Current and Future Techniques,
619 Water 14(3) (2022) 448, https://doi.org/10.3390/w14030448
620 [2] C.Y. Tang, Z. Yang, H. Guo, J.J. Wen, L.D. Nghiem, E. Cornelissen, Potable Water
621 Reuse through Advanced Membrane Technology, Environ. Sci. Technol. 52(18)
622 (2018) 10215-10223, https://doi.org/10.1021/acs.est.8b00562.
623 [3] F. Liu, N.A. Hashim, Y. Liu, M.R.M. Abed, K. Li, Progress in the production and
624 modification of PVDF membranes, J. Membr. Sci. 375(1) (2011) 1-27,
625 https://doi.org/https://doi.org/10.1016/j.memsci.2011.03.014.
626 [4] J.A. Kharraz, A.K. An, Patterned superhydrophobic polyvinylidene fluoride (PVDF)
627 membranes for membrane distillation: Enhanced flux with improved fouling and
628 wetting resistance, J. Membr. Sci. 595 (2020) 117596,
629 https://doi.org/https://doi.org/10.1016/j.memsci.2019.117596.
630 [5] J. Guo, M.U. Farid, E.-J. Lee, D.Y.-S. Yan, S. Jeong, A. Kyoungjin An, Fouling
631 behavior of negatively charged PVDF membrane in membrane distillation for
632 removal of antibiotics from wastewater, J. Membr. Sci. 551 (2018) 12-19,
633 https://doi.org/https://doi.org/10.1016/j.memsci.2018.01.016.
634 [6] W. Deng, T. Fan, Y. Li, In situ biomineralization-constructed superhydrophilic and
635 underwater superoleophobic PVDF-TiO_2 membranes for superior antifouling
636 separation of oil-in-water emulsions, J. Membr. Sci. 622 (2021) 119030,
637 https://doi.org/https://doi.org/10.1016/j.memsci.2020.119030.
638 [7] K. Samree, P.-u. Srithai, P. Kotchaplai, P. Thuptimdang, P. Painmanakul, M.
639 Hunsom, S. Sairiam, Enhancing the antibacterial properties of PVDF membrane by
640 hydrophilic surface modification using titanium dioxide and silver nanoparticles,
641 Membranes 10(10) (2020) 289, https://www.mdpi.com/2077-0375/10/10/289.
642 [8] Y. Wang, Q. Li, W. Miao, P. Lu, C. You, Z. Wang, Hydrophilic PVDF membrane
643 with versatile surface functions fabricated via cellulose molecular coating, J.

644 Membr. Sci. 640 (2021) 119817,
645 https://doi.org/https://doi.org/10.1016/j.memsci.2021.119817.
646 [9] Y.-C. Lin, G.-L. Zhuang, P.-F. Tasi, H.-H. Tseng, Removal of protein, histological
647 dye and tetracycline from simulated bioindustrial wastewater with a dual pore size
648 PPSU membrane, J. Hazard. Mater. 431 (2022) 128525,
649 https://doi.org/https://doi.org/10.1016/j.cherd.2020.02.005.
650 [10] S. Sinha Ray, R. Dangayach, Y.-N. Kwon, Surface engineering for anti-wetting
651 and antibacterial membrane for enhanced and fouling resistant membrane
652 distillation performance, Chem. Eng. J. 405 (2021) 126702,
653 https://doi.org/https://doi.org/10.1016/j.cej.2020.126702.
654 [11] A.P. Straub, E. Asa, W. Zhang, T.H. Nguyen, M. Herzberg, In-situ graft-
655 polymerization modification of commercial ultrafiltration membranes for long-term
656 fouling resistance in a pilot-scale membrane bioreactor, Chem. Eng. J. 382 (2020)
657 122865, https://doi.org/https://doi.org/10.1016/j.cej.2019.122865.
658 [12] Y.-C. Lin, K.-M. Liu, P.-L. Chiu, C.-M. Chao, C.-S. Wen, C.-Y. Wang, H.-H. Tseng,
659 Enhancing the hydrophilicity and biofoulant removal ability of a PVDF
660 ultrafiltration membrane via π-π interactions as measured by AFM, J. Membr. Sci.
661 641 (2022) 119874, https://doi.org/https://doi.org/10.1016/j.memsci.2021.119874.
662 [13] Y.-C. Lin, C.-M. Chao, D.K. Wang, K.-M. Liu, H.-H. Tseng, Enhancing the
663 antifouling properties of a PVDF membrane for protein separation by grafting
664 branch-like zwitterions via a novel amphiphilic SMA-HEA linker, J. Membr. Sci.
665 624 (2021) 119126, https://doi.org/https://doi.org/10.1016/j.memsci.2021.119126.
666 [14] K. Nayak, B.P. Tripathi, Molecularly grafted PVDF membranes with in-air
667 superamphiphilicity and underwater superoleophobicity for oil/water separation,
668 Sep. Purif. Technol. 259 (2021) 118068,
669 https://doi.org/https://doi.org/10.1016/j.seppur.2020.118068.
670 [15] Z.-Y. Xi, Y.-Y. Xu, L.-P. Zhu, Y. Wang, B.-K. Zhu, A facile method of surface
671 modification for hydrophobic polymer membranes based on the adhesive behavior
672 of poly(DOPA) and poly(dopamine), J. Membr. Sci. 327(1) (2009) 244-253,
673 https://doi.org/https://doi.org/10.1016/j.memsci.2008.11.037.
674 [16]] X. Huang, W. Wang, Y. Liu, H. Wang, Z. Zhang, W. Fan, L. Li, Treatment of oily
675 waste water by PVP grafted PVDF ultrafiltration membranes, Chem. Eng. J. 273
676 (2015) 421-429, https://doi.org/https://doi.org/10.1016/j.cej.2015.03.086.
677 [17] F. Liu, C.-H. Du, B.-K. Zhu, Y.-Y. Xu, Surface immobilization of polymer brushes
678 onto porous poly(vinylidene fluoride) membrane by electron beam to improve the
679 hydrophilicity and fouling resistance, Polymer 48(10) (2007) 2910-2918,
680 https://doi.org/https://doi.org/10.1016/j.polymer.2007.03.033.
681 [18] W. Shao, H. Ma, T. Yu, C. Wu, Z. Hong, Y. Xiong, Q. Xie, Antifouling PVDF

682 Membrane by Surface Covalently Anchoring Functionalized Graphene Quantum
683 Dots, Ind. Eng. Chem. Res. 59(45) (2020) 20168-20180,
684 https://doi.org/10.1021/acs.iecr.0c04360.
685 [19] X.-Z. Wei, J. Yang, B.-K. Zhu, Y.-Y. Xu, G.-L. Zhang, Porous poly(vinylidene
686 fluoride) membrane modified with hyperbranched poly(amine-ester), Polym.
687 Advan. Technol. 23(5) (2012) 850-857,
688 https://doi.org/https://doi.org/10.1002/pat.1979.
689 [20] Z. Wu, J. Tian, L. Wu, C. Zhang, A hydrophilic coating capable of withstanding
690 acid and alkali to modify PVDF membrane, J. Water Process Eng. 45 (2022) 102519.
691 https://doi.org/https://doi.org/10.1016/j.jwpe.2021.102519.
692 [21] G. Zin, J. Wu, K. Rezzadori, J.C.C. Petrus, M. Di Luccio, Q. Li, Modification of
693 hydrophobic commercial PVDF microfiltration membranes into superhydrophilic
694 membranes by the mussel-inspired method with dopamine and polyethyleneimine,
695 Sep. Purif. Technol. 212 (2019) 641-649,
696 https://doi.org/https://doi.org/10.1016/j.seppur.2018.10.014.
697 [22] N. Daems, S. Milis, R. Verbeke, A. Szymczyk, P.P. Pescarmona, I.F.J. Vankelecom,
698 High-performance membranes with full pH-stability, RSC Advances 8(16) (2018)
699 8813-8827, https://doi.org/10.1039/C7RA13663C.
700 [23] Y. Zhuang, D. Li, P. Ding, Z. Xu, W. Jing, Sulfonic acid-grafted polyvinylidene
701 fluoride electrospun mats as electro-Fenton reactor membrane components, RSC
702 Advances 7(46) (2017) 29193-29199, https://doi.org/10.1039/C7RA04660J.
703 [24] X. Tang, X. Yan, Dip-coating for fibrous materials: mechanism, methods and
704 applications, J. Sol-Gel Sci. Technol. 81(2) (2017) 378-404,
705 https://doi.org/10.1007/s10971-016-4197-7.
706 [25] S.R. Ravichandran, C.D. Venkatachalam, M. Sengottian, S. Sekar, B.S.
707 Subramaniam Ramasamy, M. Narayanan, A.V. Gopalakrishnan, S. Kandasamy, R.
708 Raja, A review on fabrication, characterization of membrane and the influence of
709 various parameters on contaminant separation process, Chemosphere 306 (2022)
710 135629, https://doi.org/https://doi.org/10.1016/j.chemosphere.2022.135629.
711 [26] P. Wang, J. Ma, Z. Wang, F. Shi, Q. Liu, Enhanced Separation Performance of
712 PVDF/PVP-g-MMT Nanocomposite Ultrafiltration Membrane Based on the NVP-
713 Grafted Polymerization Modification of Montmorillonite (MMT), Langmuir 28(10)
714 (2012) 4776-4786, https://doi.org/10.1021/la203494z.
715 [27] F. Chen, X. Shi, X. Chen, W. Chen, Preparation and characterization of amphiphilic
716 copolymer PVDF-*g*-PMABS and its application in improving hydrophilicity and
717 protein fouling resistance of PVDF membrane, Appl. Surf. Sci. 427 (2018) 787-797,
718 https://doi.org/https://doi.org/10.1016/j.apsusc.2017.08.096.
719 [28] J. Lv, G. Zhang, H. Zhang, C. Zhao, F. Yang, Improvement of antifouling

performances for modified PVDF ultrafiltration membrane with hydrophilic cellulose nanocrystal, Appl. Surf. Sci. 440 (2018) 1091-1100, https://doi.org/https://doi.org/10.1016/j.apsusc.2018.01.256.
[29] I.V. Maggay, C.-J. Wu, H.-R. Guo, X.-L. Liao, C.-J. Chou, Y. Chang, Y.-F. Lin, A. Venault, Superhydrophobic SiO_2/poly(vinylidene fluoride) composite membranes for the gravity-driven separation of drug enantiomers from emulsions, J. Membr. Sci. 618 (2021) 118737, https://doi.org/https://doi.org/10.1016/j.memsci.2020.118737.
[30] C. Sun, X. Feng, Enhancing the performance of PVDF membranes by hydrophilic surface modification via amine treatment, Sep. Purif. Technol. 185 (2017) 94-102, https://doi.org/https://doi.org/10.1016/j.seppur.2017.05.022.
[31] J.-H. Li, X.-S. Shao, Q. Zhou, M.-Z. Li, Q.-Q. Zhang, The double effects of silver nanoparticles on the PVDF membrane: Surface hydrophilicity and antifouling performance, Appl. Surf. Sci. 265 (2013) 663-670, https://doi.org/https://doi.org/10.1016/j.apsusc.2012.11.072.
[32] G.-d. Kang, Y.-m. Cao, Application and modification of poly(vinylidene fluoride) (PVDF) membranes – A review, J. Membr. Sci. 463 (2014) 145-165, https://doi.org/https://doi.org/10.1016/j.memsci.2014.03.055.
[33] L. Han, Y.Z. Tan, C. Xu, T. Xiao, T.A. Trinh, J.W. Chew, Zwitterionic grafting of sulfobetaine methacrylate (SBMA) on hydrophobic PVDF membranes for enhanced anti-fouling and anti-wetting in the membrane distillation of oil emulsions, J. Membr. Sci. 588 (2019) 117196, https://doi.org/https://doi.org/10.1016/j.memsci.2019.117196.
[34] S. Legeay, M. Rodier, L. Fillon, S. Faure, N. Clere, Epigallocatechin gallate: a review of its beneficial properties to prevent metabolic syndrome, Nutrients 7(7) (2015) 5443-5468, https://doi.org/10.3390/nu7075230.
[35] I. Koyuncu, B. Yavuzturk Gul, M.S. Esmaeili, E. Pekgenc, O. Orhun Teber, G. Tuncay, H. Karimi, S. Parvaz, A. Maleki, V. Vatanpour, Modification of PVDF membranes by incorporation Fe_3O_4@Xanthan gum to improve anti-fouling, anti-bacterial, and separation performance, J. Environ. Chem. Eng. 10(3) (2022) 107784, https://doi.org/https://doi.org/10.1016/j.jece.2022.107784.
[36] J.M. Yang, S.C. Tsai, Biocompatibility of epoxidized styrene–butadiene–styrene block copolymer membrane, Mater. Sci. Eng. C 30(8) (2010) 1151-1156, https://doi.org/https://doi.org/10.1016/j.msec.2010.06.014.
[37] H. Qiao, M. Chao, D. Hui, J. Liu, J. Zheng, W. Lei, X. Zhou, R. Wang, L. Zhang, Enhanced interfacial interaction and excellent performance of silica/epoxy group-functionalized styrene-butadiene rubber (SBR) nanocomposites without any coupling agent, Compos. B Eng. 114 (2017) 356-364,

https://doi.org/https://doi.org/10.1016/j.compositesb.2017.02.021.
[38] G.-L. Zhuang, H.-H. Tseng, M.-Y. Wey, Facile synthesis of CO_2-selective membrane derived from butyl reclaimed rubber (BRR) for efficient CO_2 separation, J. CO2. Util. 25 (2018) 226-234, https://doi.org/https://doi.org/10.1016/j.jcou.2018.04.003.
[39] J.-Y. Li, H.-H. Tseng, M.-Y. Wey, Tuning thermal expansion behavior and surface roughness of tubular Al_2O_3 substrates for fabricating high-performance carbon molecular sieving membranes for H_2 separation, Int. J. Hydrogen Energy. 44(45) (2019) 24746-24758, https://doi.org/https://doi.org/10.1016/j.ijhydene.2019.07.196.
[40] M. Purnima, T. Paul, K. Pakshirajan, G. Pugazhenthi, Onshore oilfield produced water treatment by hybrid microfiltration-biological process using kaolin based ceramic membrane and oleaginous Rhodococcus opacus, Chem. Eng. J. 453 (2023) 139850, https://doi.org/https://doi.org/10.1016/j.cej.2022.139850.
[41] H. Jafarian, M. Dadashi Firouzjaei, S. Aghapour Aktij, A. Aghaei, M. Pilevar Khomami, M. Elliott, E.K. Wujcik, M. Sadrzadeh, A. Rahimpour, Synthesis of heterogeneous metal organic Framework-Graphene oxide nanocomposite membranes for water treatment, Chem. Eng. J. 455 (2023) 140851, https://doi.org/https://doi.org/10.1016/j.cej.2022.140851.
[42] T.C.A. Ng, Z. Lyu, Q. Gu, L. Zhang, W.J. Poh, Z. Zhang, J. Wang, H.Y. Ng, Effect of gradient profile in ceramic membranes on filtration characteristics: Implications for membrane development, J. Membr. Sci. 595 (2020) 117576, https://doi.org/https://doi.org/10.1016/j.memsci.2019.117576.
[43] N. Debnath, A. Kumar, T. Thundat, M. Sadrzadeh, Investigating fouling at the pore-scale using a microfluidic membrane mimic filtration system, Sci. Rep. 9(1) (2019) 10587, https://doi.org/10.1038/s41598-019-47096-6.
[44] G.R. Guillen, Y. Pan, M. Li, E.M.V. Hoek, Preparation and characterization of membranes formed by nonsolvent induced phase separation: a review, Ind. Eng. Chem. Res. 50(7) (2011) 3798-3817 https://doi.org/10.1021/ie101928r.
[45] H.-H. Tseng, G.-L. Zhuang, Y.-C. Su, The effect of blending ratio on the compatibility, morphology, thermal behavior and pure water permeation of asymmetric CAP/PVDF membranes, Desalination 284 (2012) 269-278 https://doi.org/10.1016/j.desal.2011.09.011.
[46] A. Kuźmińska, D. Kwarta, T. Ciach, B.A. Butruk-Raszeja, Cylindrical polyurethane scaffold fabricated using the phase inversion method: influence of process parameters on scaffolds' morphology and mechanical properties, Materials 14(11) (2021) 2977, https://www.mdpi.com/1996-1944/14/11/2977.
[47] C. Ren, Y. Zhang, Q. Xu, T. Tian, F. Chen, Effect of non-solvent from the phase

796 inversion method on the morphology and performance of the anode supported
797 microtubular solid oxide fuel cells, Int. J. Hydrogen Energy. 45(11) (2020) 6926-
798 6933, https://doi.org/https://doi.org/10.1016/j.ijhydene.2019.12.104.
799 [48] Y.J.T. Hirai, Solvent-induced phase-inversion and electrical actuation of dielectric
800 copolymer films, Mater. Sci. Appl. 2(3) (2011) 187-195,
801 https://doi.org/10.4236/msa.2011.23023.
802 [49] C. Jin, C. Yang, F. Chen, Effects on microstructure of NiO–YSZ anode support
803 fabricated by phase-inversion method, J. Membr. Sci. 363(1) (2010) 250-255,
804 https://doi.org/https://doi.org/10.1016/j.memsci.2010.07.044.
805 [50] N. Nasrollahi, S. Aber, V. Vatanpour, N.M. Mahmoodi, Development of
806 hydrophilic microporous PES ultrafiltration membrane containing CuO
807 nanoparticles with improved antifouling and separation performance, Mater. Chem.
808 Phys. 222 (2019) 338-350,
809 https://doi.org/https://doi.org/10.1016/j.matchemphys.2018.10.032.
810 [51] J. Kazi, R. Sen, S. Ganguly, T. Jha, S. Ganguly, M. Chatterjee Debnath, Folate
811 decorated epigallocatechin-3-gallate (EGCG) loaded PLGA nanoparticles; in-vitro
812 and in-vivo targeting efficacy against MDA-MB-231 tumor xenograft, Int. J. Pharm.
813 Pharm. 585 (2020) 119449,
814 https://doi.org/https://doi.org/10.1016/j.ijpharm.2020.119449.
815 [52] Y.-C. Chiang, Y. Chang, A. Higuchi, W.-Y. Chen, R.-C. Ruaan, Sulfobetaine-
816 grafted poly(vinylidene fluoride) ultrafiltration membranes exhibit excellent
817 antifouling property, J. Membr. Sci. 339(1) (2009) 151-159,
818 https://doi.org/https://doi.org/10.1016/j.memsci.2009.04.044.
819 [53] S. Shen, Y. Hao, Y. Zhang, G. Zhang, X. Zhou, R.B. Bai, Enhancing the
820 Antifouling Properties of Poly(vinylidene fluoride) (PVDF) Membrane through a
821 Novel Blending and Surface-Grafting Modification Approach, ACS Omega 3(12)
822 (2018) 17403-17415, https://doi.org/10.1021/acsomega.8b02569.
823 [54] J. Chen, X. Meng, Y. Tian, X. Wang, J. Zhu, H. Zheng, L. Wang, Fabrication of a
824 superhydrophilic PVDF-g-PAA@FeOOH ultrafiltration membrane with visible
825 light photo-fenton self-cleaning performance, J. Membr. Sci. 616 (2020) 118587,
826 https://doi.org/https://doi.org/10.1016/j.memsci.2020.118587.
827 [55] J. Lv, G. Zhang, H. Zhang, F. Yang, Graphene oxide-cellulose nanocrystal (GO-
828 CNC) composite functionalized PVDF membrane with improved antifouling
829 performance in MBR: Behavior and mechanism, Chem. Eng. J. 352 (2018) 765-
830 773, https://doi.org/https://doi.org/10.1016/j.cej.2018.07.088.
831 [56]] F. Meng, S.-R. Chae, A. Drews, M. Kraume, H.-S. Shin, F. Yang, Recent advances
832 in membrane bioreactors (MBRs): Membrane fouling and membrane material,
833 Water Res. 43(6) (2009) 1489-1512,

834 https://doi.org/https://doi.org/10.1016/j.watres.2008.12.044.
835 [57] X. Shi, D. Li, J. Xie, S. Wang, Z. Wu, H. Chen, Spectroscopic investigation of the
836 interactions between gold nanoparticles and bovine serum albumin, Chinese Sci.
837 Bull. 57(10) (2012) 1109-1115. https://doi.org/10.1007/s11434-011-4741-3.
838 [58] N. Zhang, N. Yang, L. Zhang, B. Jiang, Y. Sun, J. Ma, K. Cheng, F. Peng, Facile
839 hydrophilic modification of PVDF membrane with Ag/EGCG decorated
840 micro/nanostructural surface for efficient oil-in-water emulsion separation, Chem.
841 Eng. J. 402 (2020) 126200,
842 https://doi.org/https://doi.org/10.1016/j.cej.2020.126200.
843 [59] J. Wu, Z. Hou, Z. Yu, J. Lang, J. Cui, J. Yang, J. Dai, C. Li, Y. Yan, A. Xie, Facile
844 preparation of metal-polyphenol coordination complex coated PVDF membrane for
845 oil/water emulsion separation, Sep. Purif. Technol. 258 (2021) 118022,
846 https://doi.org/https://doi.org/10.1016/j.seppur.2020.118022.
847 [60] Y. Sun, Y. Zong, N. Yang, N. Zhang, B. Jiang, L. Zhang, X. Xiao, Surface
848 hydrophilic modification of PVDF membranes based on tannin and zwitterionic
849 substance towards effective oil-in-water emulsion separation, Sep. Purif. Technol.
850 234 (2020) 116015,. https://doi.org/https://doi.org/10.1016/j.seppur.2019.116015.
851 [61] J. Gao, J. Wang, Q. Xu, S. Wu, Y. Chen, Regenerated cellulose strongly adhered
852 by a supramolecular adhesive onto the PVDF membrane for a highly efficient
853 oil/water separation, Green Chem. 23(15) (2021) 5633-5646,
854 https://doi.org/10.1039/D1GC01998H.